Uncertainty quantification and sensitivity analysis for the self-excited vibration of a spline-shafting system

Xinxing Ma[1], Yucai Zhong[1], Peng Cao[2], Jie Yuan[3,4], Zhenguo Zhang[1*]

[1]State Key Laboratory of Mechanical System and Vibration, Shanghai Jiao Tong University
[2]AECC Hunan Aviation Powerplant Research Institute, Zhuzhou, China
[3]Department of Mechanical and Aerospace Engineering, University of Strathclyde
[4]Department of Aeronautics and Astronautics, University of Southampton, UK

ABSTRACT

Self-excited vibrations can occur in the spline-shafting system due to internal friction of the tooth surface. However, due to manufacturing errors, design tolerances, and time-varying factors, the parameters that induce self-excited vibrations are always uncertain. This study provides new insights into the uncertainty quantification and sensitivity analysis of a spline-shaft system suffering from self-excited vibrations. The non-intrusive generalised polynomial chaos expansion (gPCE) with unknown deterministic coefficients is used to represent the propagation of uncertainties in the rotor dynamics, which allows rapid estimation of the statistics of the non-linear responses. Furthermore, the global sensitivity analysis of the stochastic self-excited vibration response of the rotor system with probabilistic uncertain parameters is evaluated by Sobol indices. The relative influence of different random parameters on the vibration behavior and initial displacement conditions for the occurrence of self-excited vibration is investigated. The accuracy of the adopted method based on the gPCE metamodel is validated by conventional Monte Carlo simulation (MCS). Finally, the effects of parameter uncertainties considering random distribution characteristics on the stochastic vibration characteristics of the rotor system are discussed, which demonstrates the need to consider input uncertainties in analysis and design to ensure robust system performance.

1. INTRODUCTION

The spline coupling is a widely used joint structure in high-speed rotatory machineries such as gas turbines, aircraft engines, and automotive drivelines [1, 2]. However, the mechanical discontinuity characteristics of splines cause interfacial friction between components within them [3, 4]. Interfacial friction is the main source of non-linearity in such systems, which can lead to complex system dynamics such as resonance frequency shift and amplitude-dependent damping, and even self-excited vibration [5]. In the practical in-service environment, the coefficient of friction usually varies with torque and misalignment as well [3], and it is not easy to analyze the friction mechanism precisely because many factors are involved (e.g. lubrication, surface roughness, load, and temperature, etc). In addition, these factors are affected by manufacturing error, design tolerance, and time-varying factors, making this type of dynamical system highly nonlinear and uncertain. Therefore, it is significantly important to ensure the reliable prediction of stability analysis and self-excited vibration by considering the nonlinear and uncertain characteristics of such systems.

In most cases, the current studies on the vibration of the spline-rotor systems have been conducted for deterministic systems. Internal damping in spline couplings is widely

* Corresponding author: zzgjtx@sjtu.edu.cn

considered to be the main cause of self-excited vibration in spline-rotor systems [6-9]. The study in Ref.[10] systematically elucidated the mechanism of axial spline friction damping in aero-turbine power plants. The results show that rotational instability occurs when the spline rotor system operating speed exceeds the critical speed. To explain the internal damping mechanism, a mathematical model of damping coefficients for predicting self-excited vibrations is developed in [11]. And it is shown in [12] that anisotropic supports can reduce the limit cycle oscillation (LCO) amplitude caused by internal damping. The literature [13] explores the effect of rubber seal damping on the self-excited vibrations of the system. In addition, the interface interaction of the splined coupling complicates the dynamics of the shaft system due to contact, clearance, wear, misalignment, etc. Work in the literature has shown how design parameters affect the mechanical characteristics of spline couplings and their impact on rotor dynamics (such as load distribution [14-17], fretting wear [18, 19], misalignment [20-22], nonlinear stiffness [23-26] and their effects on rotor dynamics [27-29]). For example, Barrot et al. [16] analytically studied the axial torque transmission characteristics in spline couplings while Hong et al. [17] proposed a generalized semi-analytic load distribution model applicable to involute splines of all common types of side-fit. Curà and Mura [22] developed the numerical model to predict the reaction moments of misaligned spline couplings and performed experimental tests to account for the effect of misalignment angle, transmitted torque, and tooth stiffness. Yu et al. [25] proposed a novel analytical stiffness model considering tooth engagement and highlighted the softening nonlinearity of the spline rotor through rotor dynamics analysis. The above literature shows that spline couplings introduce some non-linearities into the rotor system which may be potential conditions for instability. Nonetheless, most studies have focused only on the nonlinear dynamics of the spline coupling excitation and have not paid sufficient attention to the uncertainty of the system parameters.

Indeed, the internal friction occurring in splined couplings is difficult to characterize precisely from the perspective of tribology. On the one hand, in terms of grease lubrication spline, with the operation of the machine, the loss or leakage of grease and other factors will make the tooth surface lubrication in a time-varying state. On the other hand, installation errors, nicked, worn, or dirty mounting faces, loose mounting bolts, and components that exceed specified tolerances collectively contribute to high misalignments. Therefore, the relative speed of the tooth fit and the state of motion change all the time and there is a certain dispersion in the friction coefficient and misalignment. The combined effect of these parameters leaves the state of the spline coupling in a state of uncertainty. In addition, most studies assume that all the key teeth in a spline fit share the load equally whereas in reality the number of engaged teeth is much smaller than the total number of teeth and also has indeterminate characteristics depending on the load. Most studies consider the number of spline meshing teeth as a constant, e.g. Cedoz et al [30] consider the number of meshing teeth as 50% while Niemann [31] considers the number of meshing teeth as 75%. Considering the engagement sequence and load variation, Kenneth W. Chase [32] proposed a new prediction model of tooth engagement based on statistics. Therefore, there are also obvious uncertainties in spline tooth engagement, and there are few relevant studies. Rao et al [33] investigated a reliability-based design method for automotive transmission systems by considering the length of splines, transmission power, speed, and material properties as random variables. In short, the aforementioned studies indicate the high sensitivity of the dynamic behavior of friction systems to design parameters. The

sensitivity is not nearly reflected in the variation of stability, but also in the amplitude of friction-induced self-excited vibrations. Therefore, it is necessary to determine the amplitude of the friction-induced self-excited vibrations and their sensitivity to each random parameter to know if the amplitude is too large and to determine if the random parameter can be neglected.

To date, stochastic studies of friction-induced self-excited vibration have been carried out in many application scenarios, such as the study of drum brake squeal vibration [34-36]. However, it is clear from the literature survey that although a large number of publications focus on vibrations of spline-rotor systems, to the best of the authors' knowledge, the uncertainties associated with self-excited vibrations of spline-shaft systems have not been reported. On the one hand, an efficient method is needed to propagate the uncertainties of random vibrations of spline-shaft systems to friction-induced vibrations. On the other hand, the importance of each uncertain parameter on the dynamic response of spline-shafting systems needs to be investigated. Therefore, based on the fact that self-excited vibrations of splined shaft systems are naturally random and uncertain, we applied the theory of uncertainty quantification and global sensitivity analysis to this research work. In this paper, we work on extending the problem of self-excited vibration of splined shaft systems to a non-linear uncertainty statistical space using the well-established gPCE metamodel approach to ensure reliable prediction of self-excited vibration response. From the engineering design/operating point of view, the method based on the gPCE metamodel allows for fast estimation of the statistics of the non-linear rotor dynamics response and can be used for parametric analysis of the system. And the dispersion and randomness of the amplitude of friction-induced self-excited vibrations in spline-shaft systems are emphasized through such an application study. More importantly, based on the Sobol global sensitivity analysis, the key parameters affecting the self-excited vibration response in different frequency ranges are identified, which can provide some reference value for the self-excited vibration control of spline-shafting systems.

The paper is structured as follows: Section 2 is devoted to the theoretical description of the system and the methodology of uncertainty quantification. First, the governing equations of the spline-shafting system are briefly introduced. Then, the gPCE formulation and sensitivity analysis of the stochastic responses for the spline-shafting is derived. The stochastic responses are presented and discussed in section 3, where the effects of uncertain parameters are analyzed and validated by MCS. Finally, the conclusions are summarised in section 4.

2. Theoretical formulation

In this section, a brief description of the spline-shafting system is given and the system equations of motion are derived. A mathematical model of the angular misalignment of the coupling is then given. Finally, the framework for uncertainty quantification of the stochastic vibration response of the system is established and extended to sensitivity analysis.

2.1 Modeling of the spline-shafting system

2.1.1 The spline-shafting system

The physical model studied in this paper is consistent with the model in Ref. [29]. A brief description of the model is as follows. As shown in Fig.1 (a), the three-dimensional

model of the spline-shafting system is supported by the rolling bearing. The driving conical gear shaft is connected to the thin-walled long shaft by the involute external spline and the laminated membrane coupling. The length of the thin-walled rotating shaft and its connected external spline are L_r (2150mm) and L_s (156mm) respectively. The material of the rotating shaft is an aluminum alloy with a density of 2770 kg m^{-3} and an inner radius of 50 mm and an outer radius of 52 mm; the material of the spline coupling is steel with a density of 7800 kg m^{-3} and an inner radius of 35 mm and an outer radius of 50 mm.

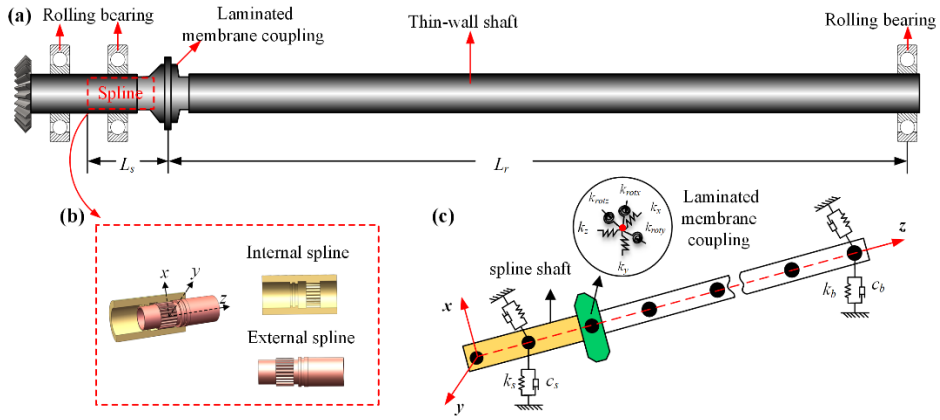

Fig. 1. (a) The three-dimensional model of the spline-shafting system (b) The sectional view of the spline coupling and its components (c) the finite element model of the spline-shafting system

Figure 1(b) is the sectional view of the spline joint which consists of the external spline and the internal spline. The lateral movement of the splines is restricted by two locating surfaces. In particular, the external spline is allowed to slide axially for a certain distance. The external spline shaft is assumed to be supported by an isotropic linear spring and damper equivalent to the spline coupling, and the membrane coupling is simplified to a linear spring in the 6 degrees of freedom(DOF) direction, see Fig. 1(c). The support parameters of the splined shaft system are given in Table 1. For a detailed description of the system, the reader is invited to refer to [29].

Table 1 Support parameters of the spline-shafting system

Physical parameter	Value
Support stiffness k_s (N/m) and support damping c_s (N·s/m) of spline coupling	2×10^7, 100
Support stiffness k_b (N/m) and support damping c_b (N·s/m) of bearing	4×10^6, 100
Support stiffness k_x, k_y, and k_z (N/m) of laminated membrane coupling	1×10^9, 1×10^9, 7×10^4
Angular stiffness k_{rotx}, k_{roty}, and k_{rotz} (N·m/rad) of laminated membrane coupling	1×10^6, 1×10^6, 7×10^6

2.1.2 The equations of motion of the spline-shafting system

The shaft is modeled with a Finite Element Model (FEM) composed of sixty Timoshenko beam elements. The elementary element contains two nodes, each with six degrees of freedom, i.e. three lateral displacements and three rotations. The interested readers can find the detailed formulation of beam element in [37].

The equation of motion of the *i*th undamped element writes:

$$\mathbf{M}_e^i\ddot{\mathbf{q}}_e^i + \omega\mathbf{G}_e^i\dot{\mathbf{q}}_e^i + \mathbf{K}_e^i\mathbf{q}_e^i = \mathbf{0} \quad (1)$$

where $\mathbf{M}_e^i$, $\mathbf{K}_e^i$, and $\mathbf{G}_e^i$ are the mass matrix, stiffness matrix and gyroscopic matrix, respectively, for the *i*th Timoshenko beam element.

Note that the axial and angular stiffness of ball bearings is ignored, and bearings and spline coupling are simplified as isotropic spring damping elements. The stiffness, k_b, and damping, c_b, matrices of the rolling bearing elements are written as

$$\begin{cases} \mathbf{K}_b = \mathrm{diag}\left[k_{bx}, k_{by}, k_{bz}, k_{brotx}, k_{broty}, k_{brotz}\right] \\ \mathbf{C}_b = \mathrm{diag}\left[c_{bx}, c_{by}, c_{bz}, c_{brotx}, c_{broty}, c_{brotz}\right] \end{cases} \tag{2}$$

The general global matrices are assembled by summing the contributions of the different components (i.e. the rotor shaft, the coupling, the flexible bearing supports, the unbalance force, and the non-linear terms). The global equation of motion of the FEM of the rotor system is then given by

$$\mathbf{M}_\mathrm{r}\ddot{\mathbf{q}}_\mathrm{r} + (\mathbf{C}_\mathrm{r} + \omega\mathbf{G}_\mathrm{r})\dot{\mathbf{q}}_\mathrm{r} + \mathbf{K}_\mathrm{r}\mathbf{q}_\mathrm{r} + \mathbf{B}_\mathrm{r}(\mathbf{q}_\mathrm{r}, \omega, t) = \mathbf{F}_\mathrm{r}(\omega, t) + \mathbf{T}_\mathrm{m} \tag{3}$$

where $\mathbf{M}_\mathrm{r}$, $\mathbf{K}_\mathrm{r}$, $\mathbf{C}_\mathrm{r}$, and $\mathbf{G}_\mathrm{r}$ are the mass, stiffness, Rayleigh damping, and gyroscopic matrices of the rotor-bearing system, respectively; ω is the rotational speed of the rotor; $\mathbf{q}_\mathrm{r}$, $\mathbf{F}_\mathrm{r}$, $\mathbf{B}_\mathrm{r}$, and $\mathbf{T}_\mathrm{m}$ are the displacement vector, unbalance force, the non-linear friction bending moment and misalignment moment respectively.

The damping $\mathbf{C}_\mathrm{r}$ is directly applied with proportional damping to the system equations. The specific formula is illustrated as follows [38]:

$$\mathbf{C}_\mathrm{r} = \alpha\mathbf{M}_\mathrm{r} + \beta\mathbf{K}_\mathrm{r} \tag{4}$$

whereα and β are the ratio coefficients, and they can be determined from any two orders of the rotor natural frequency and modal damping ratio obtained from modal experiments. For the current study, only a residual unbalanced mass is located at the center of the long shaft, i.e. the unbalance force acts only on its central node. The unbalance force $\mathbf{F}_\mathrm{r}$ can be represented as follows:

$$\mathbf{F}_\mathrm{r}^\mathrm{m}(\omega, t) = [m_\mathrm{e} e\omega^2 \cos(\omega t + \phi) \quad m_\mathrm{e} e\omega^2 \sin(\omega t + \phi) \quad 0 \quad 0 \quad 0 \quad 0]^\mathrm{T} \tag{5}$$

where m_e and e are the mass unbalance and eccentricity, respectively. ϕ is the initial angular position of the mass with respect to the rotary axis. ω defines the rotational speed of the rotor.

The expression for the bending moment due to friction in the fixed coordinate system is as follows

$$\mathbf{B}_\mathrm{r} = \begin{cases} B_x = \dfrac{2\mu T}{\pi\cos\psi} \dfrac{\Delta\dot{\theta} + \Omega\Delta\phi}{\sqrt{\Delta\dot{\beta}_x^2 + \Delta\dot{\beta}_y^2}} \\ B_y = \dfrac{2\mu T}{\pi\cos\psi} \dfrac{\Delta\dot{\phi} - \Omega\Delta\theta}{\sqrt{\Delta\dot{\beta}_x^2 + \Delta\dot{\beta}_y^2}} \end{cases} \tag{6}$$

where the $\Delta\theta$ and $\Delta\phi$ are the relative angular displacements in the fixed coordinate system and can be obtained directly by time step integration. And T, μ, and Ω are the steady transmission torque, the friction coefficient, and the rotational speed respectively. Interested readers can find the detailed formulation of this bending moment in [29].

2.1.3 Mathematical model for the misaligned rotor

Due to the low stiffness of the membrane coupling, a large angular deflection is allowed. Therefore, it can be assumed that the angular misalignments are concentrated at the membrane coupling. Figure 2 shows the angular deflection between the external spline shaft and the connecting shaft. A schematic diagram of the torque components at the

coupling is shown in Fig. 3. The line AB is the center line of the external spline shaft, and the spatial position angle of the connecting shaft relative to the external spline shaft is β, which is the angle between the projection axis and the y-axis. The input torque T can be divided into two components after passing through the elastic membrane coupling:

$$T_z = T\cos\alpha, \quad T_s = T\sin\alpha \tag{7}$$

where T_z and T_s are the torques along the connecting shaft axis and perpendicular to the connecting shaft axis, respectively.

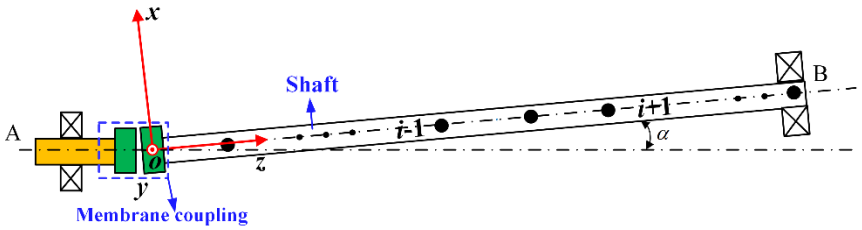

Fig. 2. Diagram of the deviation between the external splined shaft and the connecting shaft

T_s can cause lateral shaft bending deformation, which is further decomposed along the x and y axes to obtain:

$$T_x = T\sin\alpha\cos\beta, \quad T_y = T\sin\alpha\sin\beta \tag{8}$$

According to Euler's equation of motion, T_x, T_y, and T_z can be written as

$$\begin{aligned} T_x &= I_x\dot{\omega}_x + \omega_y\omega_z\left(I_z - I_y\right) \\ T_y &= I_y\dot{\omega}_y + \omega_y\omega_z\left(I_x - I_z\right) \\ T_z &= I_z\dot{\omega}_z + \omega_y\omega_x\left(I_y - I_x\right) \end{aligned} \tag{9}$$

where I_x, I_y, and I_z are the moments of inertia about the x, y, and z axes, respectively, and ω_x, ω_y, and ω_z are the angular velocities of the connecting shaft.

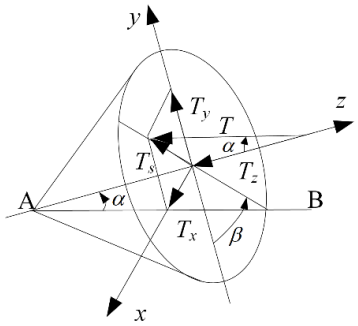

Fig. 3. Schematic diagram of equivalent misalignment moment

Since the connecting shaft rotates only about the z-axis, Eq. (9) can be reduced to

$$T\cos\alpha = I_C\varepsilon_C \tag{10}$$

where I_C represents the polar moment of inertia of the shaft and ε_C is the angular acceleration of the shaft.

The angular velocity should satisfy the following relationship [39]:

$$\frac{\omega_C}{\omega_e} = \frac{1+\mathrm{C}}{1+D\cos(2\theta_e)} \tag{11}$$

where ω_C is the angular velocity of the connecting shaft, ω_e, and θ_e are the angular velocity and angle of rotation of the external splined shaft, respectively. $\mathrm{C}=\frac{4\cos\alpha}{3+\cos 2\alpha}$, $\mathrm{D}=\frac{1-\cos 2\alpha}{3+\cos 2\alpha}$, the specific derivation of C and D can be found in Ref. 40.

The differential calculation of Eq. (11) yields

$$\frac{\varepsilon_C}{\omega_e}=\frac{2\omega_e CD\sin 2\theta_e}{(1+D\cos 2\theta_e)^2} \tag{12}$$

Thus the angular acceleration can be expressed as

$$\varepsilon_C=\frac{2\omega_e^2 CD\sin(2\omega_e t)}{[1+D\cos(2\omega_e t)]^2} \tag{13}$$

Substituting Eq. (13) into Eq. (10) yields the misalignment torque T as

$$T=\frac{2I_C\omega_e^2 CD\sin(2\omega_e t)}{\cos\alpha[1+D\cos(2\omega_e t)]^2} \tag{14}$$

2.2 Extension to the uncertain model based on the gPCE method

In this study, the Newmark β method is used to determine the steady-state solution of the friction-induced self-excited vibration. In addition, a non-intrusive probabilistic approach based on gPCE [41] is used to represent the propagation of uncertainty in the response. All uncertain parameters are assumed to be independent, and the gPCE is used to discrete the random nonlinear output S (i.e. frequency response), allowing the direct combination of uncertainty analysis and numerical integration.

Using the truncated P-term gPCE, the random representation of the response can be expressed as [41]:

$$\tilde{\mathbf{q}}(\cdot,\boldsymbol{\xi})=\sum_{i=0}^{\infty}\mathbf{g}_i\Psi_i(\boldsymbol{\xi})\approx\sum_{i=0}^{P}\mathbf{g}_i\Psi_i(\boldsymbol{\xi})=\mathbf{G}\boldsymbol{\Psi}_P(\boldsymbol{\xi}) \tag{15}$$

where $\mathbf{G}=\left[\mathbf{g}_0\quad\mathbf{g}_1\cdots\mathbf{g}_P\right]$ is the deterministic matrix of PC coefficients and $\tilde{\mathbf{g}}$ is the expansion coefficient vector, the basis vector $\Psi_i(\boldsymbol{\xi})$ is multivariate polynomial in L_2-space, which is the product of one-dimensional polynomials containing multiple indices $\left[k_{i_1}\ldots k_{i_r}\right]^{\mathrm{T}}$ and $\boldsymbol{\Psi}_P=\mathrm{d}\left[\Psi_1\quad\Psi_2\cdots\Psi_P\right]^{\mathrm{T}}$. $\Psi_i(\boldsymbol{\xi})$ can be given by the following set:

$$\Psi_i(\boldsymbol{\xi})\in\left\{\bigcup_{\mathbf{k}\in L(p)}\prod_{j=1}^{r}\psi_{k_j}\left(\xi_j\right)\right\},\forall i \tag{16}$$

where k_j is the order of the polynomial concerning the jth random variable. ψ_{k_j} denotes the univariate orthogonal polynomial. $L(p)$ denotes the multi-indexed set of full PC bases of order p:

$$L(p)=\left\{\mathbf{k}=\left[k_1\ldots k_r\right]^{\mathrm{T}}:\sum_{j=1}^{r}k_j\le p\right\},\quad\mathbf{k}_i\in L(p)\forall i$$

The dimensionality of the unknown coefficients can be represented by r and p as

$$P+1=\binom{r+p}{p}=\frac{(r+p)!}{r!\,p!} \tag{17}$$

The random polynomials are orthogonal in L2 space according to the Wiener-Askey scheme, i.e.

$$\left\langle \Psi_i, \Psi_j \right\rangle = \int_{\Omega_\xi} \Psi_i(\xi)\Psi_j(\xi) f(\xi) d\xi = \delta_{ij} \left\langle \Psi_i, \Psi_i \right\rangle \tag{18}$$

where $\Omega_\xi = \xi_1 \otimes \xi_2 \otimes \cdots \xi_r$ denotes the space of random event $\boldsymbol{\xi}$. $\langle \cdot, \cdot \rangle$ is the inner product, δ_{ij} is the Kronecker delta, and $f(\boldsymbol{\xi})$ can be given by the joint probability density function of $\boldsymbol{\xi}$ as

$$f(\xi) = \frac{1}{(\sqrt{2\pi})^r} \mathrm{e}^{\frac{1}{2}\xi^T \xi} \tag{19}$$

Taking the inner product of Eq. (15) to be $\Psi_k(\boldsymbol{\xi})$ and using the orthogonality of the polynomial basis, the unknown coefficients $\tilde{\mathbf{g}}_k$ can be obtained as follows:

$$\mathbf{g}_k = \frac{\left\langle \tilde{\mathbf{q}}, \Psi_k \right\rangle}{\left\langle \Psi_k, \Psi_k \right\rangle} = \frac{\int_{\Omega_\xi} \tilde{\mathbf{q}}(\cdot, \boldsymbol{\xi}) \Psi_k(\boldsymbol{\xi}) f(\boldsymbol{\xi}) \mathrm{d}\boldsymbol{\xi}}{\left\langle \Psi_k, \Psi_k \right\rangle}, \forall k \tag{20}$$

In practice, the integral calculation can be implemented by a Gaussian product with fast convergence and high approximate accuracy, which can be redefined as :

$$G_k = \int_{\Omega_\xi} \tilde{\mathbf{q}}(\cdot, \boldsymbol{\xi}) \Psi_k(\xi) f(\xi) \mathrm{d}\boldsymbol{\xi} \approx \sum_{l=1}^{p} \left[\bar{A}_l \tilde{\mathbf{q}}\left(\cdot, \xi^l\right) \Psi_k\left(\xi^l\right) \right] \tag{21}$$

where $\boldsymbol{\xi}_l$ and A_l are the quadrature points and weights, respectively.

A general linear system can be constructed to determine the PC coefficient once G_k has been determined:

$$\mathbf{G}^S = \mathbf{q} \begin{bmatrix} \tilde{A}_{1,0} \Psi_0^{(1)} & \tilde{A}_{1,1} \Psi_1^{(1)} & \cdots & \tilde{A}_{1,P} \Psi_P^{(1)} \\ \tilde{A}_{2,0} \Psi_0^{(2)} & \tilde{A}_{2,1} \Psi_1^{(2)} & \cdots & \tilde{A}_{2,P} \Psi_P^{(2)} \\ \vdots & \vdots & \vdots & \vdots \\ \tilde{A}_{H,0} \Psi_0^{(H)} & \tilde{A}_{H,1} \Psi_1^{(H)} & \cdots & \tilde{A}_{H,P} \Psi_P^{(H)} \end{bmatrix} \tag{22}$$

where $\mathbf{q} = \left[\mathbf{q}\left(\xi^1\right) \mathbf{q}\left(\xi^2\right) \cdots \mathbf{q}\left(\xi^l\right) \right]^{\mathrm{T}}$, $\Psi_j^{(k)} = \Psi_j\left(\xi^k\right)$, and $\tilde{A}_{i,j} = \bar{A}_i / \left\langle \Psi_j, \Psi_j \right\rangle$.

When the PC components of the responses are obtained, the estimates of the first two statistical moments (mean μ_q and variance σ_q^2) of the response $\mathbf{q}$ are given by

$$\begin{cases} \bar{\boldsymbol{\mu}}_q = E[\tilde{\mathbf{q}}(\cdot, \bar{\boldsymbol{\xi}})] \approx \mathbf{g}_0 \\ \bar{\boldsymbol{\sigma}}_q^2 = \int_{\Omega_\xi} \left[\tilde{\mathbf{q}}(\cdot, \bar{\boldsymbol{\xi}}) - \bar{\boldsymbol{\mu}}_q \right]^2 f(\bar{\xi}) \mathrm{d}\bar{\xi} \approx \sum_{i=1}^{P} \mathbf{g}_i \odot \mathbf{g}_i \left\langle \Psi_i^2 \right\rangle \end{cases} \tag{23}$$

In this work, Hermite chaos is chosen for Gaussian random variables according to the Wiener-Askey scheme. It is worth noting that this work can be easily extended to other types of random distributions of uncertain variables (e.g. lognormal or uniform distributions). This can be achieved by converting non-Gaussian probability models into equivalent Gaussian variables through uncertainty transformation.

2.3 Global sensitivity based on the Sobol method

To quantify the degree of influence of random parameters on the response of friction-induced self-excited vibration, the variance-based Sobol sensitivity index is used to analyze the global sensitivity of uncertain parameters [42]. It is obtained by decomposing the variance of the response into the sum of the contributions of each variable and their combination. The decomposition of the Sobol function for any output quantity $S(\cdot, \boldsymbol{\xi})$ can generally be given as

$$S(\cdot,\boldsymbol{\xi}) = \sum_{\beta\subseteq[1,2,\cdots,r]} S_\beta\left(\boldsymbol{\xi}_\beta\right) \tag{24}$$

where $S(\cdot, \xi)$ is any element in vector $\boldsymbol{S}$, $\beta \subseteq [1,2,\cdots,r]$ refers to any subset of integers, $\boldsymbol{\xi}_\beta = [\xi_1, \xi_2, \cdots, \xi_{\beta n}]$ with n being the number of elements in β.

The intermediate projection of Eq. (23) onto the basis of gPCE and the construction of the Sobol decomposition of gPCE by rearrangement of Eq. (23) as

$$S(\cdot,\xi) = \sum_{\beta\subseteq[1,2,\cdots,r]} S_\beta\left(\xi_\beta\right) \approx \sum_{\beta\subseteq[1,2,\cdots,r]} \sum_{k\in L(\beta)} g_k \Psi_k(\xi) \tag{25}$$

where g_k is the k-th expansion coefficient with respect to the output quantity $\boldsymbol{q}$. $L(\beta) \subset L(p)$ is the subset of indices that can be written as

$$L(\beta) = \left\{ k \in \{1,\cdots,P\} \mid \Psi_k(\bar{\xi}) = \prod_{j=1}^{r} \psi_{k_{\beta_j}}\left(\xi_{\beta_j}\right), k_{\beta_j} \geq 1 \right\} \tag{26}$$

Obviously, each term of the polynomial function in Eq. (25) depends only on the random parameters $\boldsymbol{\xi}_\beta$. Therefore, the corresponding conditional variance can be given directly as:

$$\bar{\sigma}_\beta^2 = \int_{\Omega_{\bar{\xi}}} S_\beta\left(\xi_\beta\right)^2 f\left(\xi_\beta\right) \mathrm{d}\xi_\beta \approx \sum_{k\in L(\beta)} \left(g_k\right)^2 \left\langle \Psi_k^2 \right\rangle \tag{27}$$

Estimating Sobol's Sensitivity Indices can then be approximated as follows

$$\bar{S}_\beta = \frac{\sigma_\beta^2}{\bar{\sigma}_q^2} \approx \frac{\sum_{k\in L(\beta)} \left(g_k\right)^2 \left\langle \Psi_k^2 \right\rangle}{\sum_{k=0}^{P} \left(g_k\right)^2 \left\langle \Psi_k^2 \right\rangle} \tag{28}$$

when the set β includes only one element $\{i\}$, $\bar{S}_\beta$ measures the sensitivity with regards to the random parameter ξ_i alone. Multiple-term indices, e.g. $S_{ij,\ i\neq j}$, is used to determine the sensitivity of the response variance caused by the interaction which cannot be decomposed into the contributions of those variables separately.

In addition, the total sensitivity index including the individual effects of ξ_i and their interactions with all other stochastic parameters in $\boldsymbol{\xi}$ can be easily obtained by

$$\bar{S}_T^i = \sum_{\bar{L}(\beta,i)} S_\beta\left(\bar{\boldsymbol{\xi}}_\beta\right), \quad \bar{L}(\beta,i) = \{\beta \subseteq \{1,2,\cdots,r\} : i \in \beta\} \tag{29}$$

However, this definition is not feasible for practical computations as it would require computing each index individually, which is not efficient. Instead, the sensitivity measure can be represented by all variables except variable x_i as $S_{\sim i}$, where $S_{\sim i}=S_{\boldsymbol{v}}$, $\boldsymbol{v}= \{1, ..., i-1, i+1, ..., N\}$, N is the number of input variables. So the total index can be written as:

$$\bar{S}_T^i = 1 - S_{\sim i} \tag{30}$$

3. Results and discussion

The deterministic response of a system is the basis for understanding the stochastic response analysis, therefore, this section first gives the deterministic response analysis of the system under several simple parameter conditions, emphasizing the need to consider parameter uncertainty. Subsequently, the stochastic self-excited vibration response characteristics of the system are carried out under mono-parameter and multi-parameter

respectively. Finally, the parameter correlations are elucidated by means of sensitivity curves.

3.1 Model validation

In this section, the modal information of the original deterministic system is first provided to facilitate the interpretation of the subsequent results of the self-excited vibration response. The natural frequencies and corresponding vibration modes of the system are given in Table. 2 and Fig. 4, respectively. The results show that the first- and second-order bending frequencies of the system are 59.2 Hz and 195.68 Hz, respectively, and the second-order bending frequency is much higher than the first-order bending frequency. The operating speed of the system is between the first-order critical speed and the second-order critical speed.

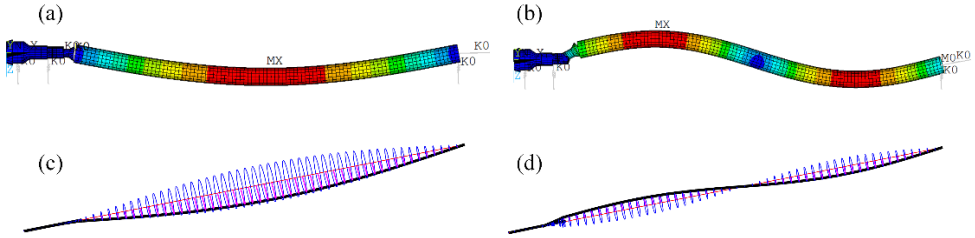

Fig. 4. Mode shapes of the system: (a) 1st order and (b) 2nd order bending mode shape by the ANSYS; (c) 1st order and (d) 2nd order bending mode shape by the developed model

3.2 System deterministic study

In order to facilitate the understanding of the uncertain response of the subsequent nonlinear self-excited system, the deterministic response analysis of a linear system in the absence of self-excitation and a nonlinear self-excited system respectively is carried out. The steady-state run-up amplitude-frequency response of the system and the corresponding three-dimensional spectrum are shown in Fig. 5. As can be seen from Fig. 5(a), there are two resonance peaks in the amplitude-frequency curve with frequency points of 29.5 Hz and 59.5 Hz, corresponding to points A and B in the spectrum Fig. 5(b). Among them, 59.5Hz is the resonance peak of the system's 1st-order natural frequency of the system, and 29.5Hz is about 1/2 of it, which is the frequency excited by the misalignment. In the three-dimensional spectrum, it can be seen that as the rotational speed increases, there is a 1 ×RPM excited by unbalance and 2 ×RPM excited by misalignment. Figure 5(c) shows that the amplitude-frequency response before the 1st-order critical speed is almost the same as in Fig. 5(a). When frictional self-excitation is considered, the rotor amplitude suddenly increases sharply and remains at large vibration amplitudes after crossing the critical rotational speed (at 65.5 Hz) is passed. The corresponding spectrum also shows a first-order natural frequency that does not vary with rotational speed after the supercritical speed, indicating the occurrence of self-excited vibration.

To clearly show the difference between the self-excited vibration response and the vibration response of the system under normal operating conditions, the shaft orbits and displacement time histories are selected for comparison under the operational rotation frequency of 75Hz. The specific results are shown in Fig. 6. Figure 6(a) shows a figure of eight shapes, which is typical of trajectories containing misalignment errors, while Fig. 6(b) shows a winding circle of the shaft trajectory, which is a limit cycle oscillation. The corresponding time histories show that the waveforms in the x and y directions of the

misalignment response differ greatly, with a distorted sine wave in the y direction, while the time domain waveform of the limit ring oscillation approximates a sine wave.

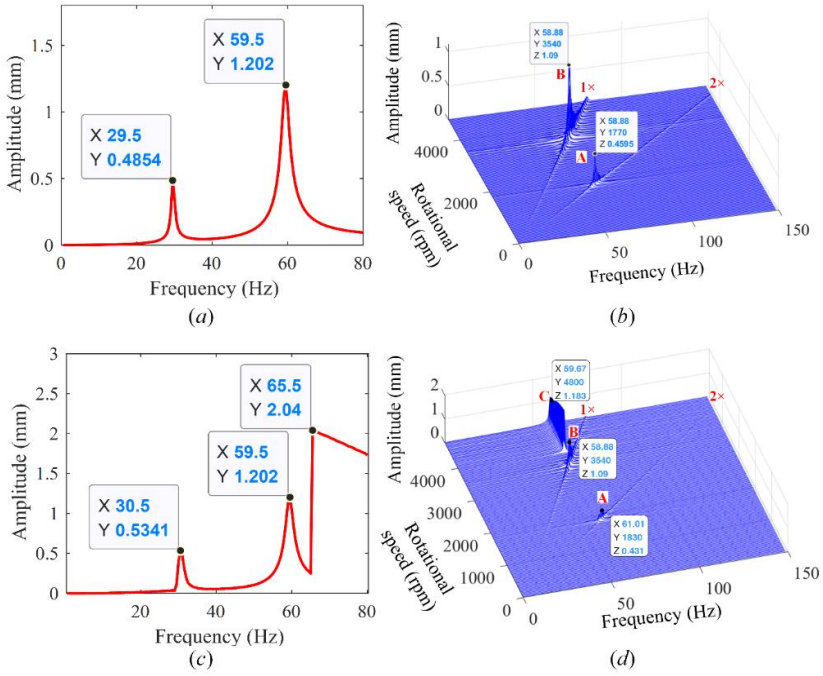

Fig. 5. (a) The run-up amplitude-frequency response and (b) three-dimensional spectrum under the shaft unbalance excitation; (c) The run-up amplitude-frequency response and (d) three-dimensional spectrum under the shaft unbalance and self-excited excitation.

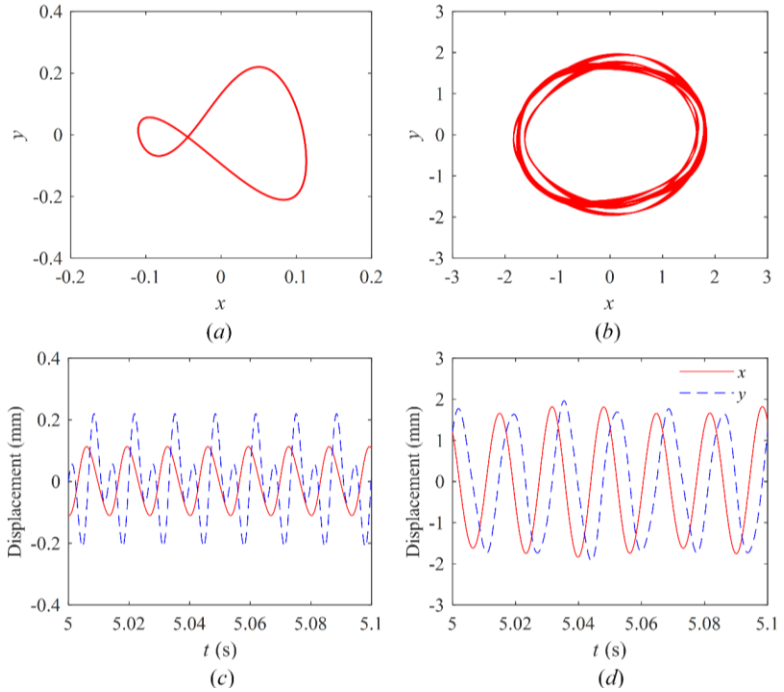

Fig. 6. Shaft orbits of (a) misaligned response and (b) self-excited vibration response; Displacement versus time plot of (c) misaligned response and (d) self-excited vibration response .

3.3 Mono-parameter uncertainty quantization

Since the misalignment angle, the friction coefficient, the load torque, and the unbalance can all change significantly in actual operating conditions, especially in the presence of faults or load variations. To further investigate the effect of uncertain parameters on the self-excited vibration characteristics of the splined shaft system, four mono-parameter (α, μ, T, and u) uncertainty analysis cases are first performed. The uncertainty is quantified for the random response of the rotor system with uncertain parameters. It is worth emphasizing that the coefficients of variation for the following individual uncertain parameters are chosen as 20% and the mean values of the misalignment angle, friction coefficient, load torque, and unbalance are 4 °, 0.15, 300 N/m, 200 g·mm. In each case, all of the parameters follow a Gaussian distribution, and 95% confidence intervals are estimated. For detailed parameter uncertainty configurations and definitions, see Ref. [35]. Furthermore, it is important to highlight that the current study's scope can be readily expanded to encompass other forms of random distributions, such as lognormal or uniform distributions, in order to accommodate uncertain variables. This expansion can be achieved by employing suitable hypergeometric polynomials based on specific statistical laws according to the Wiener-Askey scheme [41, 42], or by utilizing uncertainty transformation techniques like the Rosenblatt transformations to convert the non-Gaussian probability model into an equivalent Gaussian variable. Additionally, the current study has the potential for seamless expansion to tackle high-dimensional issues involving additional sources of uncertainty. However, it is worth noting that this paper primarily focuses on assessing the validity and feasibility of employing the gPCE metamodel to address the uncertain nonlinear self-excited vibration. Therefore, only the primary parameters affecting the self-excited vibration of the rotor system are considered random, while the complexities of high-dimensional input problems are not further explored.

3.3.1 Case 1–Uncertainty in the misalignment angle

Firstly, an uncertainty analysis is performed on the stochastic response of a spline-shafting system with an uncertain misalignment angle. In this case, the statistical amplitude-frequency response of the intermediate node of the shaft and the statistical response amplitude at the operating frequency of 75 Hz are discussed respectively. The specific results are shown in Fig. 7. The conventional MCS based on the finite element model with a sample size of 2000 and the MCS based on the gPCE metamodel with the same sample size are calculated separately. 95% confidence bounds for the amplitude-frequency response of the shaft, including the upper and lower bounds, are determined from the calculated results based on gPCE metamodel and are shown as solid blue lines. In yellow are the results of the frequency response curves for conventional MCS, which are dense and overlap each other due to a large number of samples. The mean curves obtained by gPCE are plotted alongside the conventional MCS results. The mean curve obtained by gPCE metamodel is shown as a red dashed line and the mean curve calculated by conventional MCS is shown as a black dotted line. The two mean curves have consistent trends and approximate amplitudes. The envelope based on the gPCE surrogate model contains almost all the MCS results, which verifies the accuracy of the adopted gPCE metamodel for stochastic response prediction. It can be seen that the angular misalignment variation directly leads to significant random vibration changes in the misalignment-

induced resonance band and the steady-state self-excited vibration amplitude in the amplitude-frequency curve, while the response amplitude at other frequency points is almost unchanged. It is noteworthy that the frequency point at which self-excited vibration occurs (about 64.5 Hz, the inflection point in the curve where the amplitude increases almost vertically) also remains almost unchanged. This indicates that the angular misalignment in the dynamic model established in this paper does not affect the frequency at which the self-excited limit cycle occurs, but does affect the amplitude of the limit cycle. Figure 7(b) shows the histogram of the vibration response distribution of the rotating shaft at the operating rotational frequency of 75 Hz. To illustrate the probability level of nonlinear self-excited responses, the probability density curve and the histogram of the vibration response distribution of the rotating shaft at the operating rotational frequency of 75 Hz obtained from the gPCE metamodel and conventional MCS, respectively, are shown. The results are in good agreement. The self-excited vibration amplitude distribution is skewed to the right, and the maximum amplitude is mainly concentrated at about 2.15 mm.

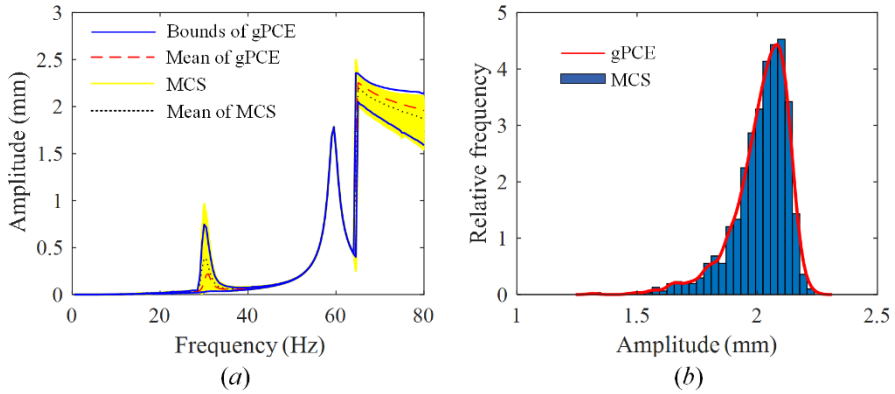

Fig. 7. (a) Statistical amplitude-frequency responses and (b) the PDFs of maximum amplitude at 75Hz with the uncertain misalignment angle

Since it is very time-consuming to calculate each sample of time-domain steady-state amplitude-frequency curves, the conventional MCS method requires a sample of amplitude-frequency curves needs to be repeatedly calculated based on the original finite element model for each parameter sampling point, which is even more costly. The gPCE method relies on evaluating the model response based on an experimental design of a small number of sample points (500 sample points in this paper) selected by the Latin hypercube sampling method [38, 43]. A surrogate model is then created based on the results of the experimental design. Finally, the thousands of samples of response results can be quickly calculated by the gPCE metamodel. Therefore, the computational efficiency is significantly improved using the gPCE metamodel compared to conventional MCS, with computation times of about 5.3 and 36 hours for gPCE and conventional MCS, respectively.

3.3.2 Case 2–Uncertainty in the load torque and friction coefficient

According to Refs. [7, 29], the frictional torque at the spline interface is positively related to the product of the friction coefficient and the load torque. Therefore, an increase in either the coefficient of friction or the load torque will directly result in an increase in the frictional torque, and the effect of the two actions is similar. Stochastic response analysis of the spline-shafting system is carried out with an uncertain coefficient of friction μ as a case study. The statistical amplitude-frequency curves obtained by the gPCE metamodel and conventional MCS methods respectively and the amplitude distribution at

the operating frequency are shown in Figs 8. It can be seen that the self-excited vibration response of the spline-shafting system occurring at supercritical rotational frequencies is significantly affected by the uncertain friction coefficient. The resonance peaks due to misalignment and unbalance excitation are hardly affected by these two variables, while the frequency point and amplitude of self-excited vibration occurrence are more variable. From the horizontal coordinate, the frequency point where self-excitation occurs is not a definite frequency, but a supercritical frequency interval, and from the vertical coordinate, the amplitude of the self-excited response evolves into an interval. The combined effect of the frequency point at which the self-excited vibration occurs and the change in amplitude leads to an envelope in the amplitude-frequency curve, the response curves from the MCS mostly fall within the envelope. In addition, the random distribution of the system response amplitude at the operating frequency of 75 Hz due to the separate variation of the frictional coefficient is shown in Figs. 8(b). The histogram distribution of the displacement amplitude and the probability density curve approximate the normal distribution.

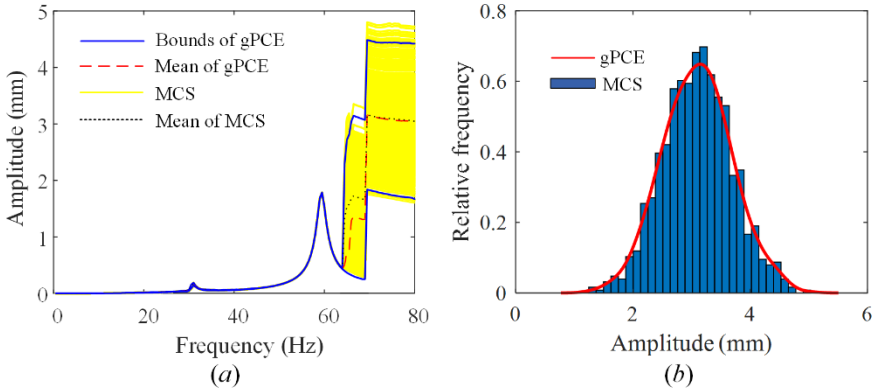

Fig. 8. (a) Statistical amplitude-frequency responses and (b) the PDFs of maximum amplitude at 75Hz with the uncertain friction coefficient

3.3.3 Case 3–Uncertainty in the unbalance

Furthermore, the uncertainty analysis for the stochastic response of the system under the variation of the unbalance u is calculated, as shown in Fig. 9. Obviously, the first resonance peak of the stochastic response is significantly affected by the uncertain unbalance, see Fig. 9(a). Since the unbalance is positively correlated with the square of the rotational speed, for the uncertain parameter u, it can be seen that for the uncertain parameter u as the rotational frequency increases (after exceeding 30 Hz), the displacement response across the frequency band increases with the increase in unbalance. The frequency points at which self-excited vibration occurs varies within [65-70] Hz with the unbalance, indicating that the self-excited instability speed threshold is significantly influenced by the unbalance. In addition, most of the amplitude-frequency curves obtained by the conventional MCS fall within the confidence bounds predicted by the gPCE-based metamodel, again confirming the validity of the surrogate model. Meanwhile, the self-excited vibration amplitude at the operating rotational frequency in Fig. 9(b) shows an approximately normal distribution with the amplitude concentrated at 2.05 mm.

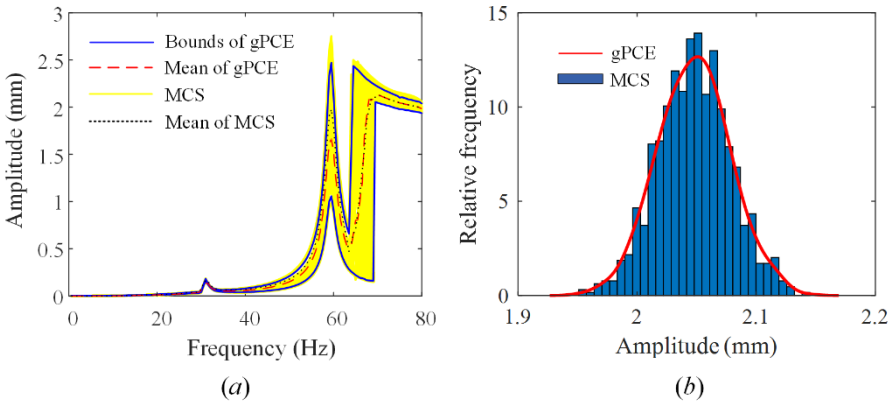

Fig. 9. (a) Statistical amplitude-frequency responses and (b) the PDFs of maximum amplitude at 75Hz with the uncertain unbalance

3.4 Multi-parameter uncertainty quantization and parameter sensitivity analysis

3.4.1 Statistical analysis of self-excited vibration response

The uncertainty analysis for the stochastic response of the spline-shafting system with multiple uncertain parameters α, μ, T, and u is performed, as shown in Fig. 10. The coefficients of variation in the multi-parameter uncertainty analysis are all chosen to be 15%. The effect of multiple uncertain parameters on the system vibration is more significant than that of a single parameter. The resonance peak due to misalignment, the 1st order resonance peak due to unbalance excitation, and the unstable rotational frequency and vibration amplitude due to self-excited vibration all change simultaneously, implying the joint influence of multiple parameters. Compared to the deterministic response, the results are no longer in a single curve but form an envelope in the global range. Figure 10(b) shows the box-and-whisker plots of three sets of amplitude responses at three typical frequency points (30 Hz at the misalignment resonance frequency, 59.5 Hz at the first-order resonance frequency, and 75 Hz at the operating rotation frequency). The medians at the three frequencies are 0.15, 1.19, and 3.06, respectively. The plots show symmetrical distribution with the median approximately equal to the mean, indicating that the system response output is approximately normally distributed. However, the range of the amplitude distribution (maximum and minimum value interval) varies considerably. It can be seen that the self-excited vibration response amplitude distribution range is the largest, and its minimum displacement amplitude can be lower than the first-order resonance peak, which is less destructive to the structural integrity, while the maximum displacement amplitude can exceed the first-order resonance peak, which is more destructive to the structural integrity.

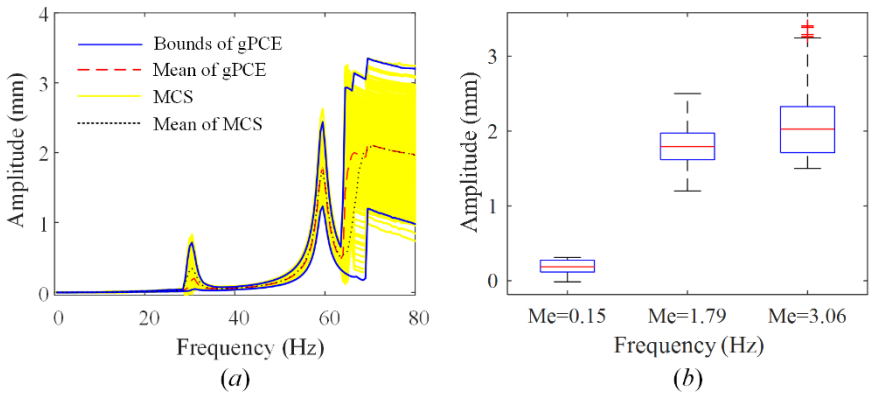

Fig. 10. (a) Statistical amplitude-frequency responses and (b) the PDFs of maximum amplitude at 75Hz with the multi-parameter uncertainty

3.4.2 Global sensitivity analysis

In this section, the global sensitivity analysis of the stochastic response of the spline-shafting system with uncertain parameters is further performed by MCS and gPCE simulations using the variance-based Sobol index. First, the accuracy of the adopted method is illustrated by the sensitivity results of the friction coefficient μ on the amplitude-frequency response of the rotating shaft displacement. Here, an example of the considered spline-shafting system with a 10% variation of all uncertain parameters is used and again the MCS with 2000 samples is used as a reference solution. Figs. 11(a) and (b) show the first-order and total sensitivity results, derived from gPCE and MCS. It can be found that these sensitivity indices are very close to each other in the frequency range of interest, which means that the adopted method has good accuracy. The sensitivity results based on the other parameters calculated by the two methods are also in very good agreement with each other, and in order to avoid repetitive descriptions, the comparison of the sensitivity indices of the other parameters is not provided.

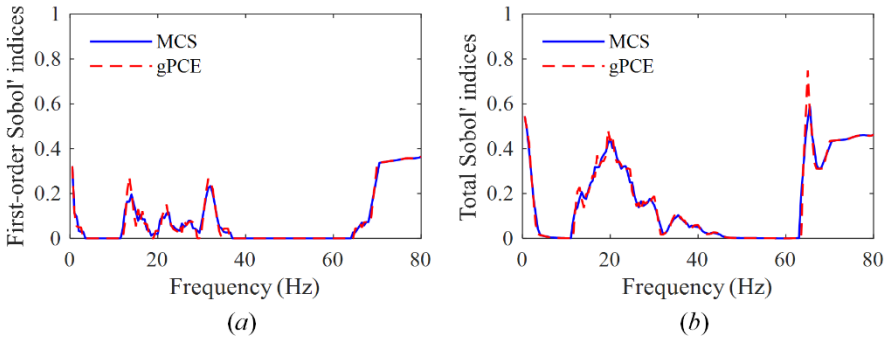

Fig. 11. Comparisons between (a) the first and (b) the total Sobol sensitivity indices of amplitude-frequency response estimated by the gPCE and MCS for the random friction coefficient

The Sobol index can be used to quantify the contribution of each uncertain parameter to the overall variance of the random response. Fig. 12(a)-(d) shows the global sensitivity of each of the four different parameters considered for the rotating shaft frequency response. It can be seen that each uncertain parameter plays an important role in the different frequency bands of the random response of the shaft. In the low-frequency range of 0-10Hz and the 1st-order resonance range of 40-60Hz, the unbalance has the greatest effect on the displacement response amplitude; in the 20-40Hz range, the effect of

the misalignment angle has the greatest effect on the response, and the other parameters also have similar effects; in the 60-80Hz range, the friction coefficient and the load torque have comparable effects on the response amplitude due to the occurrence of the self-excited response, while the unbalance and misalignment angle have minimal effects on the self-excited response amplitude. Since the product of the friction coefficient and torque affects the friction torque, the two parameters have similar effects on the system response, so the sensitivity indices trends are consistent, which supports the previous analysis of the single parameter results.

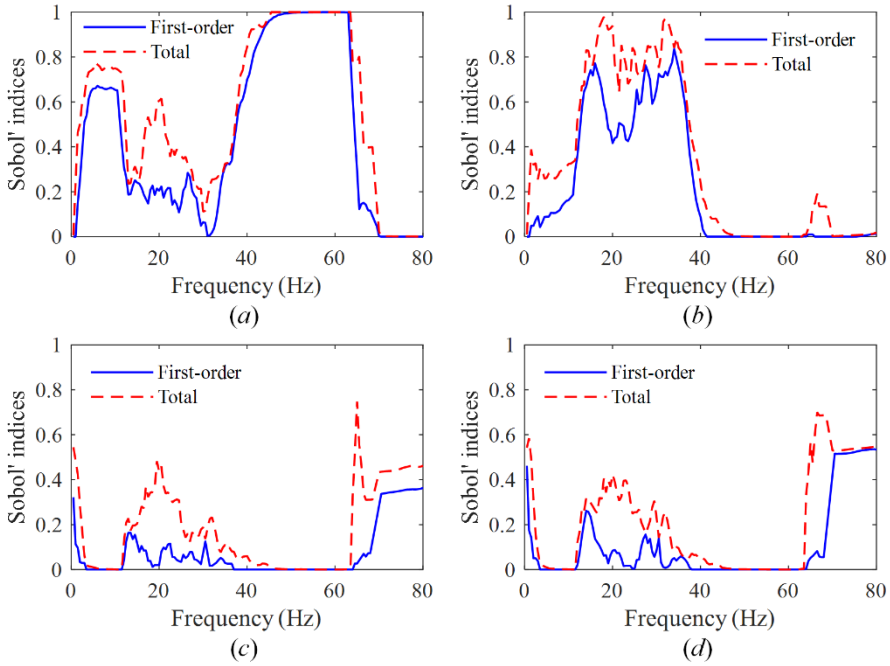

Fig. 12. Comparisons between the total (in red) and the first (blue) Sobol sensitivity indices of amplitude-frequency responses estimated by the gPCE for the random parameters (a) unbalance u, (b) misalignment angle α, (c) friction coefficient μ, and (d) load torque T

Moreover, higher-order Sobol' indices are ignored in this work. The total sensitivity is close to the 1st order sensitivity over a wide range of frequency bands, indicating that the influence of parameter coupling is globally weak. However, the total sensitivity is significantly higher than the 1st order sensitivity in the frequency range [10-36] Hz dominated by misalignment, and the frequency range [65-80] Hz where self-excited vibration occurs. The disparities observed between the total and first-order sensitivity indices in Fig. 10 indicate that interactions among the uncertain input variables contribute to a significant proportion of the system response variances. Notably, the combined effects of μ and T play a crucial role in shaping the amplitude-frequency curves within the range of [65-80] Hz, whereas the variances of amplitude-frequency curves between 10 and 36 Hz are partially attributed to the interaction effects among all four parameters. Consequently, when considering the influence patterns of uncertain parameters on the system responses, the variances of responses can be categorized into three primary groups: (i) dominantly influenced by a single parameter, (ii) independently affected by multiple parameters, and (iii) influenced by the interactions of multiple parameters. The third category presents an intriguing aspect, but it poses greater challenges in practical applications due to the non-additive nature of the combined effect of probability parameters, which indicates a distinct

interrelationship among the uncertain variables. In general, the quantitative and intuitive ranking of parameter importance on the random response, as obtained from the sensitivity curves, provides a more comprehensive understanding compared to the amplitude envelopes depicted in Figures 7-10.

3.4.3 Prediction of self-excited instability probability

It is well known that self-excited vibration systems are very sensitive to initial values. In the above-mentioned simulation of the steady-state run-up amplitude-frequency response calculation, the initial value at the initial frequency point is a very small (order of magnitude 1e-6) random number, and thereafter, as the speed increases, the final value of the current step is used as the initial value for the next calculation step for the integration iteration up to the maximum frequency point. This results in the maintenance of self-excited oscillations once they occur at some speed point in the supercritical speed interval.

However, if the initial value of the displacement is chosen randomly, the occurrence of self-excited vibration has a certain probability. A specific random initial value analysis is carried out at an operating frequency of 75 Hz, and the results are shown in Fig. 13. Figure 13(a) shows a comparison of the time domain response of the shaft for two sets of very different initial values. When the initial values are small in both directions, the shaft exhibits forced vibration, with unbalance and misalignment moments playing a major role. When the initial value is large (for example, the initial value of displacement in the *x*-direction is 0.6mm), the displacement time histories in the *x*-direction show an obvious limit cycle, and the amplitude gradually increases and eventually converges. Assuming a uniform distribution of initial values in both directions [0, 1], the traditional MCS based on the full computational model (finite element model) with a sample size of 2000 and the MCS based on the gPCE metamodel with a sample size of 10000 were calculated respectively. The statistical results based on MCS and gPCE are shown in Fig. 13(b) and (c), respectively, where the red scatter points are the initial value points where the LCO occurs and the black points are the initial value points where the LCO does not occur. The color of the scatter points is determined by the amplitude of the response. The results show a discrepancy between red and black, which is due to the fact that the response amplitudes are bipolar. The main reason for this is that the chosen steady-state solution has a long computational period, which ensures that the occurring LCO reaches a state of convergence such that its displacement amplitude is much larger than in the case of normal vibration, i.e., the response amplitude presents two extremes. The blue solid line in the figures represents the boundary between stable and unstable regions. It should be noted that the above statistical results can predict the probability of LCO occurrence, i.e., the ratio of the red scatter points to the total sample points in MCS and gPCE, which are 0.597 and 0.610, respectively. The error in the ratio obtained by these two methods is small, confirming the accuracy of predicting the probability of instability based on the gPCE model. However, the gPCE model requires far fewer sampling points than the MCS and the computational efficiency is higher.

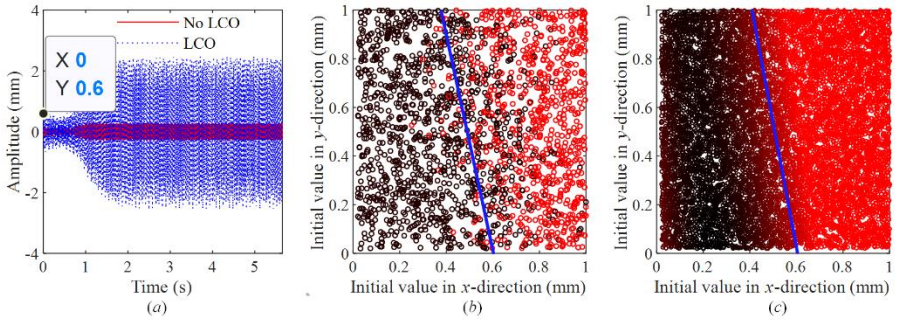

Fig. 13. (a) Time domain displacement response for two sets of different initial values (b) N=2000 samples from the region of interest labeled by their long-term behavior based on MCS (c) N=10000 samples from the region of interest predicted by gPCE model

4. Conclusions

The objective of this study is to quantify the influence of input uncertainties on the self-excited vibration of the spline-rotor system. It aims to characterize the stochastic amplitude-frequency response and the global sensitivities of these uncertain input parameters, to finally determine the probability of self-excited instability under different initial value conditions. A non-linear stochastic model for the uncertainty and sensitivity analysis of a spline-shafting system is first established. Unbalance, misalignment, friction coefficient, and load torque are considered the main uncertain resources in the system modeling, and the stochastic amplitude-frequency response under mono- and multi-parameter uncertainties is efficiently obtained using a non-intrusive gPCE model. The results show that these uncertainties can lead to significant fluctuations in the amplitude and frequency of the self-excited vibration occurrence of the spline-shaft system. The global sensitivity analysis is then performed to identify the importance of each uncertain parameter and its contribution to the variation of the frequency response. Finally, statistical analysis under different initial value conditions clarifies the probability of the possible occurrence of self-excited instability. These results are also compared with those of conventional MCS, demonstrating the computational efficiency and effectiveness of the adopted method. The applied research in this paper has highlighted the amplitude dispersion and randomness of friction-induced self-excited vibrations of the spline-shaft systems, obtaining more realistic phenomena and, more importantly, as the key parameters affecting self-excited vibrations in different frequency intervals have been identified through Sobol-based global sensitivity analysis. It provides a deeper understanding of the self-excited vibration response and provides useful guidance for the design process of the spline-shafting system.

ACKNOWLEDGMENT

The authors gratefully acknowledge the support provided by the National Natural Science Foundation of China (NSFC, Grant No. 51975354 and 5211101941). Jie Yuan also acknowledges the support from the Royal Society (Grant No. IEC\NSFC\211005)

REFERENCES

[1] Hong, J., Talbot, and D., Kahraman, A., 2014, “Load distribution analysis of

clearance-fit spline joints using finite elements", Mech. Mach. Theory, 74, pp. 42-57.
[2] Zhao, G., Zhao, X., Qian L., Yuan, Y., Ma, S., and Guo M., 2022, "A Review of aviation spline research", Lubricants, 11(1), 6.
[3] Guo, Y., Lambert, S., Wallen, R., Errichello, R., and Keller, J., 2016, "Theoretical and experimental study on gear-coupling contact and loads considering misalignment, torque, and friction influences", Mech Mach Theory, 98, pp. 242-262.
[4] Curà, F., and Mura, A., 2013, "Experimental procedure for the evaluation of tooth stiffness in spline coupling including angular misalignment", Mech Syst Signal Process, 40(2), pp. 545-555.
[5] Artiles, A. F., 1993, "The effects of friction in axial splines on rotor system stability", ASME J Eng Gas Turbines Power, 115(2), pp. 272-278.
[6] Dai, Z., Jing, J., Chen, C., and Cong, J., 2018, "Extensive experimental study on the stability of rotor system with spline coupling", ASME Turbo Expo 2018: Turbomachinery Technical Conference and Exposition.
[7] Dai, Z., Jing, J., Chen, C., Cong, J., and Quan, Y., 2023, "Analytical and experimental investigation on stability of rotor system with spline coupling considering torque, friction coefficient and external damping", Mech Mach Theory 181: 105200.
[8] Bently, D. E., and Muszynska, A., 1985, "Rotor internal friction instability". NASA. Lewis Research Center Instability in Rotating Machinery.
[9] Wang, T., Wang, Y., Liu M., and Zhong, Z., 2022, "Stability analysis of rotor with a spline coupling". Journal of Physics: Conference Series. Vol. 2252. No. 1. IOP Publishing.
[10] Walton, J., Artiles, A., Lund, J., Dill, J., and Zorzi, E., 1990, "Internal rotor friction instability". MTI 88TR39, Mechanical Technology Incorporating, Latham, NY, USA.
[11] Marmol, R. A., Smalley, A. J., and Tecza, J. A., 1980, "Spline coupling induced nonsynchronous rotor vibrations", ASME J Mech Des, 102(1), pp. 168-176.
[12] Roger Ku, C. P., Walton, J. F., and Lund Jr., J. W., 1994, "Dynamic coefficients of axial spline couplings in high-speed rotating machinery", ASME J Vib Acoust, 116(3), pp. 250-256.
[13] Zhu, H., Chen W., Zhu, R., Gao, J., and Liao, M., "Modelling and dynamic analysis of spline-connected multi-span rotor system, Meccanica, 55(6), pp. 1413-1433.
[14] Cuffaro V., Curà F., and Mura A., 2012, "Analysis of the pressure distribution in spline couplings", Proc Inst Mech Eng Part C J Eng Mech Eng Sci, 226(12), pp. 2852-2859.
[15] Curà, F., Mura, A., and Gravina, M., 2012, "Load distribution in spline coupling teeth with parallel offset misalignment", Proc Inst Mech Eng Part C J Eng Mech Eng Sci, 227(10), pp. 2195-2205.
[16] Barrot, A., Paredes, M., and Sartor, M, 2009, "Extended equations of load distribution in the axial direction in a spline coupling". Eng Fail Anal, 16 (1), 200–211.
[17] Hong, J., Talbot, D., and Kahraman A., 2015, "A generalized semi-analytical load distribution model for clearance-fit, major-fit, minor-fit, and mismatched splines", Proc Inst Mech Eng Part C J Eng Mech Eng Sci, 230(7-8), pp. 1126-1138.
[18] Curà, F., and Mura, A., 2017, "Evaluation of the fretting wear damage on crowned splined couplings, Procedia Structural Integrity 5, pp: 1393-1400.
[19] Zhao, Q., Yu, T., Pang, T., and Song, B., 2022, "Spline wear life prediction

considering multiple errors", Eng Fail Anal, 131, 105804.
[20] Xiao, L., Xu, Y., Chen, Z., and Zhang, L., 2022, "Non-linear dynamic response of misaligned spline coupling: theoretical modeling and experimental investigation", J Vib Control, 10775463211067104.
[21] Xiao, L., Xu, Y., Sun, X., Xu, H., and Zhang, L., 2022, "Experimental investigation on the effect of misalignment on the wear failure for spline couplings", Eng Fail Anal, 131, 105755.
[22] Curà, F., and Mura, A., 2014, "Experimental and theoretical investigation about reaction moments in misaligned splined couplings", Mech Syst Signal Process, 45(2), pp. 504-512.
[23] Liu, S., Ma, Y., Zhang, D., and Hong, J., 2012, "Studies on dynamic characteristics of the joint in the aero-engine rotor system", Mech Syst Signal Process, 29, pp. 120-136.
[24] Zhang, Q., Li, W., Liang, Z., and Hong, J., 2014, "Study on the stiffness loss and its affecting factors of the spline joint used in rotor systems". ASME Turbo Expo: Power for Land, Sea, and Air, Vol. 45769.
[25] Yu, P., Wang, C., Liu, Y., and Chen, G., 2022, "Analytical modeling of the lateral stiffness of a spline coupling considering teeth engagement and influence on rotor dynamics", Eur J Mech A-Solids, 92, 104468.
[26] Hong, J., Talbot, D., and Kahraman A., 2016, "A stiffness formulation for spline joints", ASME J Mech Des, 138(4), 043301.
[27] Hu, X., Hu, B., Zhang, F., Fu, B., Li, H., and Zhou, Y., 2018, "Influences of spline assembly methods on nonlinear characteristics of spline–gear system", Mech Mach Theory, 127, pp. 33-51.
[28] Xue, X., Huo, Q., Dearn, K. D., Liu, J., and Jia, J., 2021, "Involute spline couplings in aero-engine: predicting nonlinear dynamic response with mass eccentricity", Proc Inst Mech Eng Pt K-J Multi-Body Dyn, 235(1), pp. 75-92.
[29] Ma, X., Song, Y., Cao, P., Li, J., and Zhang, Z., 2023, "Self-excited vibration suppression of a spline-shafting system using a nonlinear energy sink".Int. J. Mech. Sci., 108105.
[30] Cedoz, R. W., and Chaplin, M. R., *Design Guide for Involute Splines*. Warrendale, PA: SAE, 1994
[31] Deutschman, A. D., Michels, W. J., and Wilson, C. E., 1975, *Machine Design, Theory and Practice*. Macmillan, NY.
[32] Kenneth W. Chase, Carl D. Sorensen, and Brian J.K. DeCaires, 2009, "Variation analysis of tooth engagement and loads in involute splines". IEEE Trans. Autom. Sci. Eng., 7.4, 746-754.
[33] Rao, S. S. and Tjandra, M., 1994, "Reliability-based design of automotive transmission systems". Reliab. Eng. Syst. Saf. 46.2, 159-169.
[34] Nobari, A., Ouyang, H., and Bannister, P., 2015, "Uncertainty quantification of squeal instability via surrogate modelling," Mech Syst Signal Process, 60, 887-908.
[35] Sarrouy, E., Dessombz, O., and Sinou, J. J., 2013, "Stochastic study of a non-linear self-excited system with friction". Eur J Mech A-Solids, 40, 1-10.
[36] Nechak, L., Berger, S., and Aubry, E., 2012, "Prediction of random self friction-induced vibrations in uncertain dry friction systems using a multi-element generalized polynomial chaos approach". ASME J Vib Acoust, 134(4).

[37] Tatar, A., Schwingshackl, C. W., and Friswell, M. I., 2019, "Dynamic behaviour of three-dimensional planetary geared rotor systems", Mech Mach Theory, 134, pp. 39-56.
[38] Ma, X., Zhang, Z., and Hua, H., 2022, "Uncertainty quantization and reliability analysis for rotor/stator rub-impact using advanced Kriging surrogate model", J Sound Vib, 525, 116800.
[39] Xu, M., and Marangoni, R. D., 1994, "Vibration analysis of a motor flexible coupling–rotor system subject to misalignment and unbalance, part I: theoretical model and analysis", J. Sound Vib., 176(5), 663–679.
[40] Liu, Y., Zhao, Y., Li, J., Lu, H., and Ma, H., 2020, "Feature extraction method based on NOFRFs and its application in faulty rotor system with slight misalignment". Nonlinear Dyn, 99: 1763-1777.
[41] Zhang, Z., Ma, X., Hua, H., and Liang, X., 2020, "Nonlinear stochastic dynamics of a rub-impact rotor system with probabilistic uncertainties". Nonlinear Dyn, 102, 2229-2246.
[42] Zhang, Z., Ma, X., Yu, H., and Hua, H., 2021, "Stochastic dynamics and sensitivity analysis of a multistage marine shafting system with uncertainties". Ocean Eng., 219, 108388.
[43] Yuan, J., Fantetti, A., Denimal, E., Bhatnagar, S., Pesaresi, L., Schwingshackl, C., and Salles, L., 2021, "Propagation of friction parameter uncertainties in the nonlinear dynamic response of turbine blades with underplatform dampers." Mech. Syst. Signal Proc., 156, 107673.